Available online at www.sciencedirect.com

ScienceDirect

Acta Materialia 62 (2014) 69–80

Acta MATERIALIA

www.elsevier.com/locate/actamat

Characterizing deformed ultrafine-grained and nanocrystalline materials using transmission Kikuchi diffraction in a scanning electron microscope

Patrick W. Trimby [a,*], Yang Cao [b], Zibin Chen [b], Shuang Han [c], Kevin J. Hemker [d], Jianshe Lian [c], Xiaozhou Liao [b], Paul Rottmann [d], Saritha Samudrala [b], Jingli Sun [b,e], Jing Tao Wang [e], John Wheeler [f], Julie M. Cairney [a,b]

[a] Australian Centre for Microscopy and Microanalysis, The University of Sydney, Sydney, NSW 2006, Australia
[b] School of Aerospace, Mechanical and Mechatronic Engineering, The University of Sydney, Sydney, NSW 2006, Australia
[c] Key Laboratory of Automobile Materials, Ministry of Education, College of Materials Science and Engineering, Jilin University, Nanling Campus, Changchun 130025, People's Republic of China
[d] Departments of Materials Science and Engineering and Mechanical Engineering, Johns Hopkins University, Baltimore, MD 21218, USA
[e] School of Materials Science and Engineering, Nanjing University of Science and Technology, Nanjing 210094, People's Republic of China
[f] The Department of Earth and Ocean Sciences, The University of Liverpool, Liverpool L69 3GP, UK

Received 23 August 2013; received in revised form 14 September 2013; accepted 16 September 2013
Available online 15 October 2013

Abstract

The recent development of transmission Kikuchi diffraction (TKD) in a scanning electron microscope enables fast, automated orientation mapping of electron transparent samples using standard electron backscatter diffraction (EBSD) hardware. TKD in a scanning electron microscope has significantly better spatial resolution than conventional EBSD, enabling routine characterization of nanocrystalline materials and allowing effective measurement of samples that have undergone severe plastic deformation. Combining TKD with energy dispersive X-ray spectroscopy (EDS) provides complementary chemical information, while a standard forescatter detector system below the EBSD detector can be used to generate dark field and oriented dark field images. Here we illustrate the application of this exciting new approach to a range of deformed, ultrafine grained and nanocrystalline samples, including duplex stainless steel, nanocrystalline copper and highly deformed titanium and nickel–cobalt. The results show that TKD combined with EDS is a highly effective and widely accessible tool for measuring key microstructural parameters at resolutions that are inaccessible using conventional EBSD.
© 2013 Acta Materialia Inc. Published by Elsevier Ltd. All rights reserved.

Keywords: Nanocrystalline; Ultrafine grained; Severe plastic deformation; Transmission Kikuchi diffraction; Electron backscatter diffraction

1. Introduction

Nanocrystalline, nanostructured and ultrafine-grained (UFG) materials offer properties that are vastly different from and often superior to those of the conventional microcrystalline materials [1,2]. Improvements include, but are not limited to, higher strength and hardness [3–6], enhanced fatigue resistance (B.L. Boyce, unpublished research; see also Ref. [7]), greater diffusivity, superior magnetic properties [8,9], and self-healing of radiation-induced damage through the absorption and recombination of point defects [10]. Nanocrystalline thin films, membranes, laminates, and coatings are becoming ubiquitous in micro- and nanoscale structures and devices. In contrast, processing limitations have slowed the widespread introduction of bulk structural materials, but grain size refinement by severe plastic deformation (SPD), primarily

* Corresponding author. Tel.: +61 2 9351 7561; fax: +61 2 9351 7682.
E-mail address: patrick.trimby@sydney.edu.au (P.W. Trimby).

1359-6454/$36.00 © 2013 Acta Materialia Inc. Published by Elsevier Ltd. All rights reserved.
http://dx.doi.org/10.1016/j.actamat.2013.09.026

through equal channel angular pressing (ECAP) and high-pressure torsion (HPT) [11–14], have received much attention and hold considerable promise. Grain size refinement by SPD has the extra benefit of introducing additional nanoscale structures into the material, including dislocation substructures, nanotwins, and nanoscale precipitates, all of which can further improve the material's mechanical strength [15,16].

Detailed understanding of the processing–structure–property relations in these UFG and nanocrystalline materials requires quantitative characterization on the grain and subgrain scale, which poses a significant challenge. Transmission electron microscopy (TEM) is the most widely applied technique for studying nanocrystalline materials. TEM has the necessary spatial resolution, and electron diffraction analysis enables the measurement of crystallographic orientations on the nanometre scale, and recent developments in automated electron diffraction systems utilizing precession techniques [17,18] show much promise in enabling rapid collection of orientation maps on truly nanocrystalline materials. However, TEM analyses require significant technical expertise and are relatively difficult to perform. Moreover, the physical requirements of TEM make in situ testing significantly harder than they are by scanning electron microscopy (SEM). Many published analyses of nanocrystalline materials are based on interpretations of bright and dark field (DF) TEM images [19,20]; whilst clearly showing the dislocation structures, it is very difficult to determine effectively true grain sizes on the basis of such images because many estimations of grain size are all too often representations of intragranular cell structures with relatively low lattice misorientations.

For many fine grained and UFG materials SEM-based orientation mapping with electron backscatter diffraction (EBSD) has become the characterization technique of choice. EBSD enables the rapid measurement of phase and crystallographic orientations from polished surfaces of bulk materials, with sub-micrometre spatial resolution [21–23]. EBSD can also be used simultaneously with energy dispersive X-ray spectroscopy (EDS) to characterize the chemistry of a sample, albeit with poorer spatial resolution (typically of the order of 1–5 μm). SEM is also a versatile imaging platform, and the high sample tilt required for EBSD analyses is ideal for acquiring channelling (or orientation) contrast images using forescatter detectors mounted below the EBSD detector phosphor screen [24]. However, the spatial resolution of the EBSD technique is limited by the acceleration voltage of the incident electron beam and the atomic number of the sample: the best absolute resolution figures recorded for EBSD analyses on Cu are of the order of 30 nm, and for Al 100 nm [21,25,26], with significantly worse resolution down the tilted sample surface. These figures are mostly achieved using lower accelerating voltages in order to reduce the diffraction pattern source volume: however, reducing the accelerating voltage makes diffraction pattern collection slower and increases the influence of sample contamination and drift. It is clear that conventional EBSD is not an ideal technique for characterizing truly nanocrystalline materials. Even coarser grained, severely deformed samples are challenging to measure using EBSD, as the high dislocation density results in blurred or non-existent diffraction patterns and very low indexing rates.

In the last 1–2 years there has been significant interest in and development of an alternative electron diffraction technique using SEM, namely transmission Kikuchi diffraction (TKD) [27,28], sometimes referred to as transmission EBSD (t-EBSD), although technically it does not utilize backscatter diffraction. TKD involves the analysis of electron transparent samples, similar to those prepared for TEM work, and the collection of Kikuchi patterns projected from the underside of the sample using a conventional EBSD detector. The advantage of the TKD technique over conventional EBSD is the significant improvement in spatial resolution, shown to be in the range 2–10 nm for a range of materials. Trimby [28] demonstrated the potential of TKD in the SEM (SEM-TKD) for the routine automated analysis of nanostructured samples, and a number of recent publications have shown applications of this new technique [29–32]. However, many of these data sets were relatively small, or showed significant problems with the data quality, including numerous unindexed points, indexing errors or sample drift.

In this paper we demonstrate the power of SEM-TKD for characterizing microstructures of UFG and nanocrystalline materials that have undergone deformation, including several that have been severely plastically deformed, and discuss the impact that this accessible technique will have on our understanding of material deformation on the nanoscale.

2. Materials and methodology

2.1. Materials

Four different samples were chosen to illustrate the efficacy of characterizing nanoscaled materials with TKD. These materials cover a range of materials, microstructures and processing histories. The details of each sample are described below.

2.1.1. Nanocrystalline copper

A bimodal nanocrystalline Cu sample was produced using electron beam evaporation, creating a 200 nm thick Cu film on a photoresist substrate. The substrate was then etched away using acetone. The mean grain size of the nanocrystalline matrix produced using this technique was measured (by TEM image analysis) as 39 nm, with 26.1% of the area accounted for by coarser grains that had a mean grain size of 361 nm. The film was then strained at room temperature using a high-accuracy load cell to a final strain of 2.5% at a strain rate of $5 \times 10^{-6}\ s^{-1}$. Subsequent TEM analysis indicated a slight coarsening of the grain size in the nanocrystalline matrix to 45 nm.

2.1.2. Duplex stainless steel

The steel sample is a commercial DP3W duplex stainless steel in the form of rectangular plates. It has a composition of C 0.017, Si 0.3, Mn 0.5, P 0.015, S 0.001, Ni 7.0, Cr 25, Mo 3.3, W 2.0 and N 0.28 (wt.%), and has approximately equal volume fractions of the body-centred cubic (bcc) ferrite (α) phase and the face-centred cubic (fcc) austenite (γ) phase [33]. The steel plates were first cut into discs with a diameter of ~9.8 mm and a thickness of ~1.7 mm. The discs were then ground using 800 and 1200 grit sandpaper to obtain a smooth surface and a uniform thickness of ~0.8 mm to be ready for HPT processing. A quasi-constrained HPT machine [14] was used to process the discs at room temperature and under conditions of 6 GPa for 2 and 16 revolutions at a rate of 1 r.p.m. Discs were marked to check for slippage during HPT, and the results indicated no apparent slippage up to six revolutions. The equivalent von Mises shear strain can be calculated to be approximately 37 and 297 at the edge of the 2R and 16R samples, respectively.

2.1.3. Titanium

The Ti sample used in this study was a hexagonal close-packed (hcp) α-Ti plate containing minor impurities, including O 0.08, H 0.01, N 0.01, C 0.005, Fe 0.035 (wt.%). The as-received hot rolled plate was annealed at 1073 K for 1 h. A cylindrical sample with a diameter of 10 mm and a height of 15 mm was cut from the annealed plate and was then subjected to dynamic plastic deformation (DPD) at a strain rate of 10^2–10^3 s^{-1} at room temperature and to a final deformation strain of 1.6. The DPD process involved placing the cylinder on a lower anvil and compressing it using an upper impact anvil at a high loading rate in a dynamic compression facility, with multiple impacts required to reach the desired strain [31,34,35]. Discs to be made into TEM foils were cut from the centre of the sample in a plane containing the compression axis, as described by Sun et al. [31].

2.1.4. Nickel–cobalt alloy

This dual phase Ni–Co sample was produced using electro-chemical deposition, which resulted in an initial mean grain size of 16 nm and a composition of Ni 33.3, Co 66.7 (wt.%) [36]. The sample was then deformed in compression using a Hopkinson Bar at room temperature to a strain of 0.48 at a strain rate of 2800 s^{-1}.

2.2. Sample preparation

The steel, Ti and Ni–Co samples were prepared for TEM analysis in a standard way; machining 3 mm diameter foils and then electropolishing the samples with a Struers TenuPol 5 electropolisher until a central perforation was observed. Additional thinning and cleaning was performed using a Gatan Precision Ion Polishing System (PIPS), equipped with a cold stage, to ensure a relatively large electron transparent area. The Cu film was already electron transparent, but brief thinning of the film was carried out using the PIPS to produce regions <100 nm in thickness. All of the results presented here were collected on samples with thicknesses estimated to be in the range 50–100 nm. These estimates were made from TEM studies of the same samples and, in the case of the steel, sectioning and measurement of the foil thickness using a focused ion beam scanning electron microscope.

2.3. Experimental set-up

2.3.1. Transmission Kikuchi diffraction

The samples were mounted in a custom built Al TEM sample holder that clamped individual TEM foils at a tilt of 20° from horizontal. The holder was mounted onto the stage in a Carl Zeiss Ultra Plus field emission gun (FEG) scanning electron microscope, and the stage was then tilted to 20°. This resulted in the samples being in a horizontal position in the microscope chamber, as shown in Fig. 1. The 20° stage tilt also ensured that no part of the stage was positioned under the electron beam, eliminating problems associated with backscattered electrons scattering from the stage itself and affecting the TKD pattern quality. Some previous studies have used back tilted TEM foils [27,30], but we found no benefit in this set-up. Indeed, the horizontal position of the samples removes the need for any dynamic focus or tilt correction, improves the spatial resolution (by minimizing the through sample thickness) and ensures that the sample is in an optimal position for simultaneous EDS analysis. The sample was positioned at a short working distance (5–7 mm), so that it was just above the level of the top of the EBSD detector phosphor screen (Fig. 1). The electron beam energy was set to 30 kV for all the analyses, except for the Ti sample for which 25 kV was used (in order to increase the diffracted signal for this lower atomic number material). The beam current was typically set to 1–10 nA, with maximized depth of field ("High Current" mode on the Carl Zeiss FEG

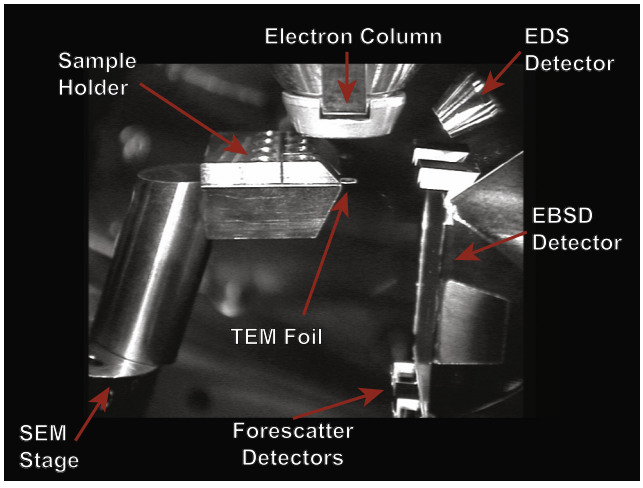

Fig. 1. In-chamber video camera image showing the standard set-up for TKD and EDS analyses of electron transparent TEM foils.

scanning electron microscope). This last setting was essential for acquiring high-quality Kikuchi diffraction patterns from the samples. Transmitted Kikuchi diffraction patterns were imaged using a standard commercially available EBSD detector (Oxford Instruments Nordlys Nano) and were processed using the Oxford Instruments AZtec 2.0 EBSD software. No modifications to the software set-up compared with normal EBSD were required. TKD patterns were collected using image resolutions of typically 168 × 128 pixels, at acquisition speeds of 30–100 patterns per s. Orientation mapping was performed as for standard EBSD, although the spacing between measurements ("step size") ranged from 4 to 10 nm, far below what is effectively possible with EBSD. Indexing rates were very sample dependent, and were generally in the 70–85% range. Careful processing of the data sets was required to remove isolated indexing errors and to remove some of the unindexed points. This would typically involve two or three low-level iterations to reduce the number of non-indexed pixels plus the removal of "grains" less than 4 pixels in size. Most orientation maps were collected in 1–2 h or less, but some larger analyses with over 2 million data points have been successfully collected, taking in excess of 6 h.

Sample drift and contamination were both occasional problems encountered during the TKD analyses. For long high resolution analyses, in which orientation measurements were taken with a step size of 5 nm or less, it was beneficial to leave the system for at least 1–2 h to minimize thermal and mechanical drift and to improve the vacuum level in the microscope chamber. For shorter or for lower resolution measurements effective analyses could be started immediately.

The TKD orientation maps were processed using standard EBSD processing software, the CHANNEL software from Oxford Instruments, providing grain, phase, orientation and boundary information.

Further processing to determine dislocation information from the TKD data was carried out using the weighted Burgers vector (WBV) technique explained in Wheeler et al. [37]. The WBV is defined as the sum, over all dislocation types, of [(density of intersections of dislocation lines with a map) × (Burgers vector)] and as such can be calculated from a planar set of orientation measurements such as in an EBSD or a TKD orientation map. There is no assumption about the orientation gradient in the third dimension and the magnitude of the WBV can be calculated to provide a lower limit of the true dislocation density.

2.3.2. Dark field imaging

The forescatter detector (FSD) system available on many commercial EBSD detectors enables DF imaging of electron transparent samples. The FSD system in this case consists of four backscatter electron (BSE) diodes positioned around the EBSD detector phosphor screen, two above the screen and two below. The lower two diodes combine to provide a good DF image of the sample, highlighting thickness variations, density contrast and some channelling contrast. In this mode the FSD system is extremely useful for finding suitably thin regions of the sample for subsequent TKD analysis. However, inverting the signal from one of the lower BSE diodes and combining it with the signal from the other lower diode eliminates both the thickness and density contrast dependence, and enhances the orientation contrast. This oriented dark field (ODF) mode provides exceptionally useful images of the microstructure, even in samples with significant variations in thickness. Examples of both types of FSD DF image are shown in Fig. 2.

2.3.3. Energy dispersive X-ray analyses

The chemistry of the samples was characterized using an Oxford Instruments AZtec EDS system with an X-Max 20 mm^2 silicon drift detector. Spectra were collected from every TKD measurement point simultaneously with TKD mapping, with no penalty on the acquisition speed. Typically 50–100 X-rays were measured from each point, enough to build up element maps for the major constituent elements. This EDS system was set up for standard SEM analyses on bulk samples, and so the matrix corrections in the EDS software were not optimized for the analysis of electron transparent samples. This restricted EDS measurements to qualitative analyses, with accurate quantitative analyses only possible on thicker regions of the samples. Additional problems were caused by the aluminium sample holder used for mounting the TEM foils: many secondary X-rays fluoresced from the holder itself, and a prominent Al peak was always visible in the EDS spectra. However, the Al element map could be used to illustrate sample thickness variations. The tapered design of the TEM foil holder shown in Fig. 1 was intended to minimize these background X-rays and to maximize the proportion of X-ray signal arising from the sample.

2.3.4. Transmission electron microscopy

It is instructive to compare the images collected using the FSD system as well as the TKD orientation maps themselves with conventional TEM images. For this reason we collected both bright field (BF) and DF TEM images of the duplex stainless steel using a Philips CM12 transmission electron microscope, operating at 120 kV accelerating voltage.

3. Results

The principle aim of this paper is to demonstrate the effectiveness of the SEM-TKD technique for the characterization of deformed UFG and nanocrystalline materials, and not to focus on the interpretation of the material deformation itself. This will be published separately for the relevant samples. Therefore, the results here are presented with a view to highlighting the quantitative nanoscale characterization that can be achieved with TKD.

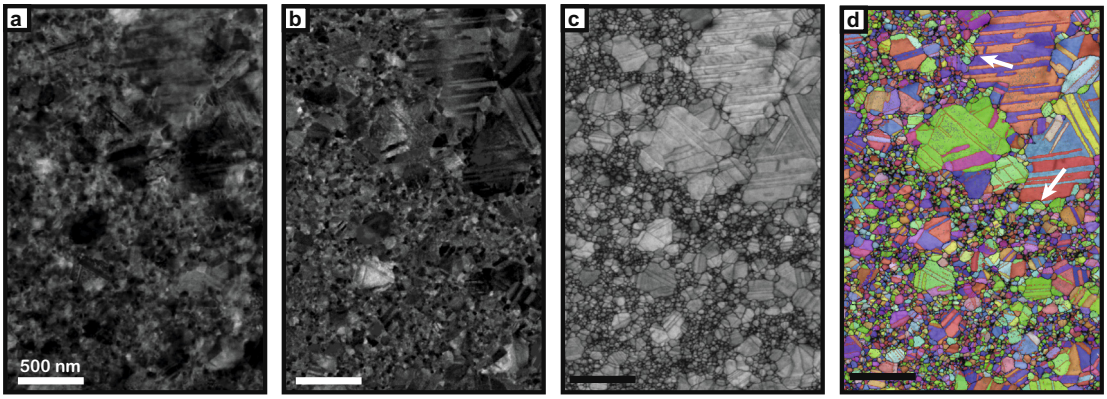

Fig. 2. TKD results from the nanocrystalline Cu sample. The scale bar in all images is 500 nm. (a) DF image collected using forescatter detectors. (b) ODF image highlighting orientation variations. (c) TKD pattern quality map of the same area. (d) TKD orientation map (inverse pole figure *z*-direction colouring), with high-angle boundaries in black, low-angle boundaries in grey and coincident site lattice boundaries in colours. White arrows mark locations showing evidence of nanocrystalline grain growth as discussed in the text. (For interpretation of the references to colour in this figure legend, the reader is referred to the web version of this article.)

3.1. Nanocrystalline copper thin film

In these samples the research aim was to test whether a bimodal grain distribution enables multiple deformation mechanisms during straining: dislocation slip in the larger grains and stress-coupled grain boundary migration in the nanocrystalline matrix. Analysis by TKD allows an assessment of the relative activity of these mechanisms, expressed as grain growth in the nanocrystalline matrix and substructure development in the larger grains.

The results of the FSD imaging and TKD analyses of one strained Cu thin foil are summarized in Fig. 2. This shows an area of 2×3 μm, mapped with a TKD step size of 4 nm. Previous TEM measurements of this sample indicate a typical sample thickness of 80 nm. The data shown here are part of a larger analysis, covering 5.5×6.5 μm. A DF image of the area collected using the FSD detectors is shown in Fig. 2a. Although the image provides some indication of the grain structure, it is difficult to visualize the general microstructural characteristics due to the contrast associated with sample thickness variations. The ODF image of the same area (Fig. 2b) removes the thickness contrast and highlights the orientation contrast. It is now clear that there is a bimodal grain size, with large (>250 nm diameter) grains containing abundant twin domains (shown by the alternating, parallel sided regions of different orientation contrast) surrounded by a nanocrystalline matrix.

The TKD pattern quality map (using the Kikuchi band contrast) in Fig. 2c shows this bimodal grain size extremely clearly. The sharpness of the grains and boundaries, even in the nanocrystalline matrix, is apparent; it is only in some of the thicker parts of the sample that the nanocrystalline matrix results in slightly poorer quality TKD patterns (darker areas in the band contrast image correlating with brighter regions in the DF image). The resulting orientation map (Fig. 2d) shows excellent indexing in all areas of the analysis region. The red lines (Σ3 twin boundaries) are abundant in both the larger grains, as expected from the ODF image, but also in the nanocrystalline matrix. The lack of any dominant colour in this orientation map indicates that there is no preferred orientation of either the larger grains or the grains in the matrix. There appears little evidence for significant development of dislocation structures in the larger grains, as expressed by low-angle boundaries in the 2–10° misorientation range. However, there are a number of places where grains in the nanocrystalline matrix appear to have grown at the expense of large grains, indicative of grain boundary migration. Two such examples are marked with arrows in Fig. 2d. Grain size measurements in the matrix regions (here classified as all grains below 100 nm diameter, excluding Σ3 and Σ9 coincident site lattice boundaries) give a mean grain size of 38.1 ± 0.4 nm, a little below the 45 nm size determined by TEM following deformation. The precise reason for this discrepancy in measured grain size is unclear and further investigation into the grain sizes of strained and as-deposited samples are ongoing, using both TEM and TKD measurements.

3.2. Duplex stainless steel

The main aim of the research into HPT-deformed duplex stainless steels has been to characterize the microstructure developing during high-strain, room-temperature deformation and subsequent grain size refinement. Of particular interest are the phase distribution, the nature of the grain, twin and low-angle boundaries and the grain size, as all of these parameters have a significant impact on the bulk material properties (e.g. strength, ductility and corrosion resistance).

TKD analyses of the HPT-deformed duplex stainless steel were carried out on both the 2 revolution (2R) and 16 revolution (16R) samples, using a step size of 4 nm and analysis areas of 1×1.5 μm. For both samples areas with approximately equal amounts of α-ferrite (bcc) and

γ-austenite (fcc) were chosen. The results are summarized in Fig. 3. The TKD pattern quality maps (Kikuchi band contrast) (Fig. 3a and d) show that excellent quality patterns are obtained from the ferrite regions (shown in red in the phase maps, Fig. 3b and e), with poorer quality patterns collected from the austenite regions (blue in the phase maps). There is a noticeable decrease in the grain size of the austenitic regions compared with the ferrite, and this is also clear in the orientation maps (Fig. 3c and f). In both samples significant intragranular deformation is apparent in both phases, indicated by the presence of many low-angle boundaries (grey lines in the orientation maps) and changes in colour within individual grains.

The grain size in the austenitic regions in both samples is so small that it is at the limit of the TKD technique resolution, and there are regions that are too fine grained to allow the collection of indexable diffraction patterns. Even so, more than 50% of the austenitic regions could be indexed and this allows us to identify some important microstructural features, such as the abundance of Σ3 twin boundaries (red lines in the orientation maps) and the fact that many of the regions that appear in the pattern quality maps to have grain sizes below 30 nm are actually made up of domains separated by low-angle (<10°) subgrain boundaries. One such region is very apparent in the austenite in the 2R sample, marked with an arrow in the orientation map (Fig. 3c).

The TKD results allow a quantitative comparison between the 2R and 16R samples. For example, the grain size in the ferrite decreases from a mean of 74.7 ± 5.7 nm in the 2R sample (134 grains) to 47.7 ± 3.0 nm in the 16R sample (210 grains), and there is also a clear increase in grain alignment with increasing deformation. Likewise, the grain boundaries can be analysed quantitatively: although not shown here, the fraction of high-angle boundaries increases with increasing deformation in both the ferritic and the austenitic regions, while the proportion of resolved Σ3 twin boundaries in the austenite remains approximately constant.

A TEM BF image of the 16R sample is shown in Fig. 4a at approximately the same scale as the TKD maps in Fig. 3. This image is taken from a different area of the same sample, but also contains approximately equal areas of austenite and ferrite. The phases can be distinguished on the basis of the grain size (austenite is finer grained), but it is very difficult to evaluate with any degree of accuracy the grain size in either phase on the basis of this image. Likewise, the DF image of the same area (Fig. 4b) provides

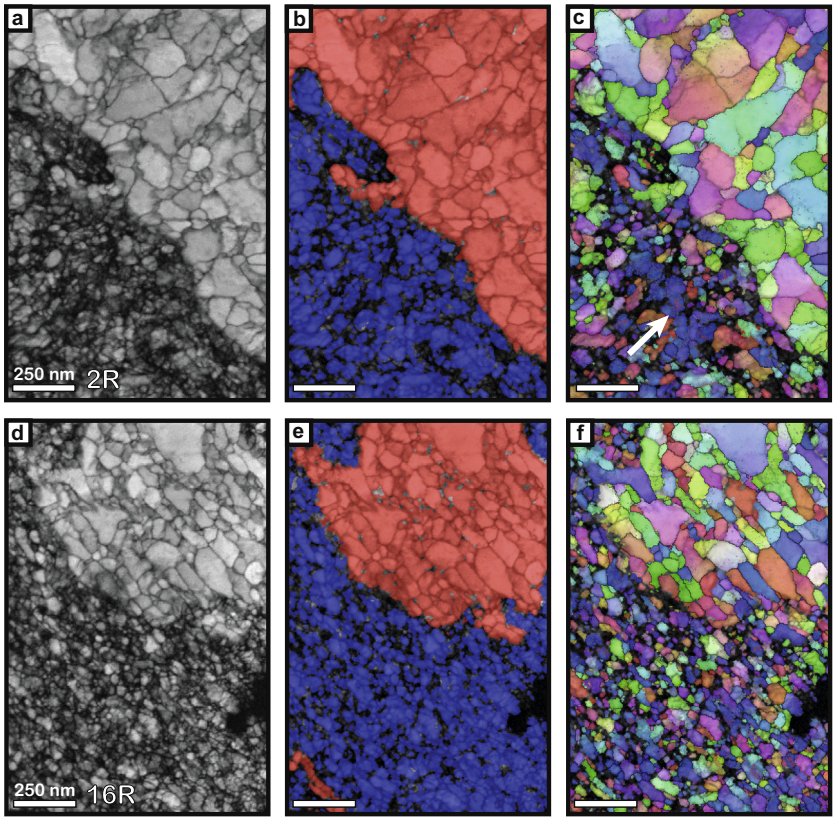

Fig. 3. TKD results from the HPT-deformed duplex stainless steel samples, comparing the (a–c) 2R sample and (d–f) 16R sample. All scale bars are 250 nm. (a, d) TKD pattern quality maps. (b, e) Phase maps, with ferrite in red and austenite in blue. (c, f) TKD orientation map (inverse pole figure *z*-direction colouring), with high-angle boundaries in black, low-angle boundaries in grey and coincident site lattice boundaries in colours. The arrow in (c) highlights a substructured grain discussed in the text. (For interpretation of the references to colour in this figure legend, the reader is referred to the web version of this article.)

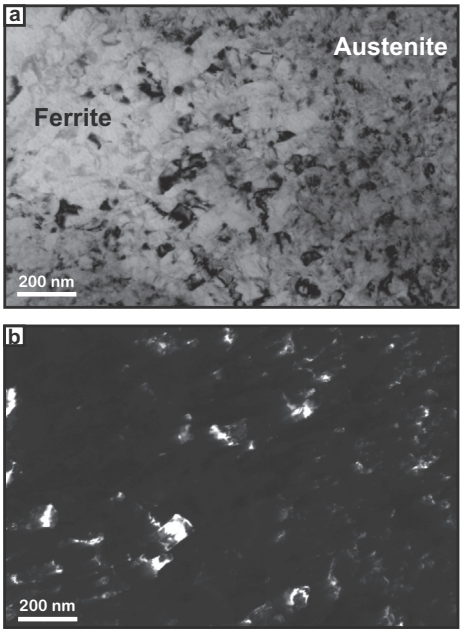

Fig. 4. TEM images of the 16R HPT-deformed duplex stainless steel sample. The right half of the image is mostly austenite, the left half ferrite (marked accordingly). (a) BF image. (b) DF image.

an indication of the grain size, but is also very difficult to interpret and does not allow an easy statistical measurement of the grain size distribution.

3.3. Titanium

In order to understand the mechanical properties of these Ti samples the nature of the deformation mechanism needs to be identified. In particular, the formation of twin boundaries, the relationship between grain orientation and dislocation density and the activity of individual slip systems are key microstructural parameters that can be measured using TKD.

The DPD-processed Ti sample was analysed using TKD with a map size of 4.1 × 5.4 μm and a step size of 10 nm. The results are summarized in Fig. 5. The TKD pattern quality map (Fig. 5a) shows that this sample is not nanocrystalline. Indeed, some of the grains appear to be greater than 1 μm in diameter, although other regions appear to be nanocrystalline. Almost all of the area shows sharp boundaries, with the exception of the top left corner of the map where the sample was significantly thicker. The orientation map (Fig. 5b) shows that many of the "nanocrystalline" grains in the pattern quality map are in fact subgrains, bounded by low-angle boundaries. Many of the grains are relatively large, >3 μm across, but they show evidence of extremely high amounts of intragranular deformation (shown either by the presence of low-angle boundaries or by significant changes in colour in the orientation map). Within some grains in this area the change in orientation exceeds 10° along 100 nm transects. Additional analyses of these deformed Ti samples have indicated the presence of abundant hcp twinning, but these twin boundaries are not shown here and are dealt with in detail elsewhere [31,32].

The magnitude of the weighted Burgers vector across the whole mapped area has been plotted in Fig. 5c. The scale shows the magnitude (μm^{-1}); there are very few areas in the whole map that have magnitudes below 0.1 μm^{-1}, which indicates that a lower bounding value for the dislocation density in this sample is in the 10^{14} m^{-2} range, with numerous regions exceeding 10^{15} m^{-2}. However, a study of the directions of the weighted Burgers vectors (not shown here) shows only a slight preference to lie in the basal plane, as might be expected if there was dominant basal slip. Further investigation shows that those weighted Burgers vectors with a magnitude >1 μm^{-1} have a stronger preference to lie in the basal plane. There appears little correlation between the orientation of individual grains and the crystallographic direction of the weighted Burgers vectors.

3.4. Nickel–cobalt alloy

For the Ni–Co it is important to understand the mechanism of grain growth during the deformation process and, in particular, the relationship between strain rate,

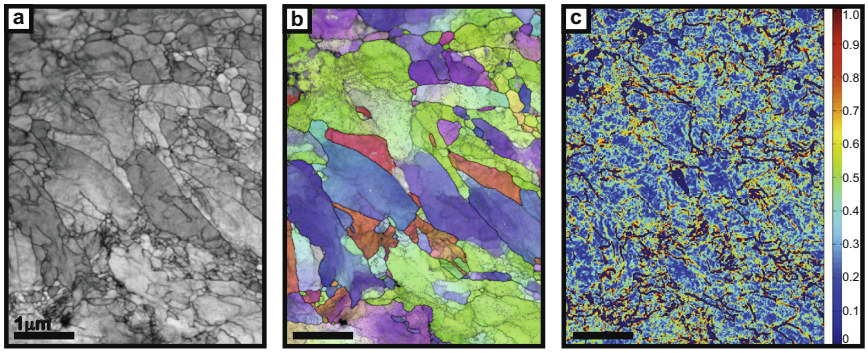

Fig. 5. TKD results from the deformed Ti sample. All scale bars are 1 μm. (a) TKD pattern quality map. (b) TKD orientation map (inverse pole figure *z*-direction colouring), with high-angle boundaries in black and low-angle boundaries in grey. (c) Weighted Burgers vector magnitude map of the same area (unit μm^{-1}). (For interpretation of the references to colour in this figure legend, the reader is referred to the web version of this article.)

texture, grain size and the nature of twin boundaries. Additionally, the influence of the composition of the starting material is of interest, including the degree and nature of any chemical segregation that may occur during deformation.

An area of the Ni–Co sample was analysed using combined TKD and EDS, covering an area of 1.5 × 3 μm with a step size of 5 nm. Although nominally a dual phase sample, all the diffraction patterns were indexed with an fcc structure and no evidence was found for an hcp phase in this region. The reason for this apparent lack of hcp phase remains unclear and further, in-depth investigations are required. The results are summarized in Fig. 6. Figs. 6a and b show the forescatter detector DF and ODF images, respectively; clearly the thickness contrast dominates the DF image, with the microstructure far more apparent in the ODF image. Long thin grains are visible in the ODF image, and these are also apparent in the TKD pattern quality image (Fig. 6c). As with the Ti sample, increasing sample thickness causes the Kikuchi pattern quality to decrease, shown by the blurred appearance in the lower third of the TKD pattern quality map. The orientation map in Fig. 6d highlights the elongated nature of many of the grains, as well as the high degree of intragranular deformation, indicated by the abundance of low-angle boundaries and the change in colour within many grains. Many of the high-angle boundaries satisfy the orientation relationship for coincident site lattice (CSL) boundaries, with abundant Σ3 and Σ11 boundaries marked in red and yellow, respectively.

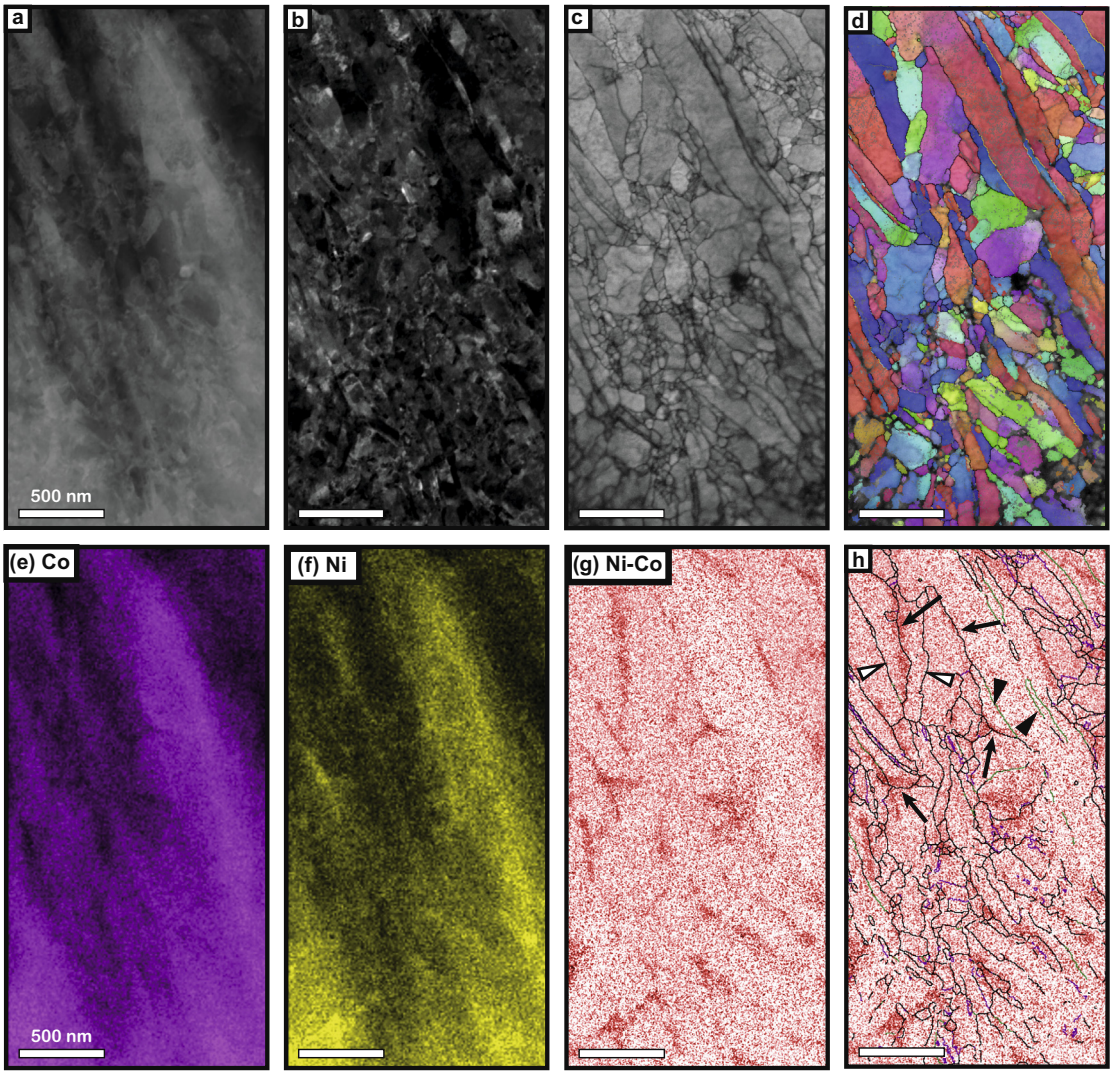

Fig. 6. TKD and EDS results from a deformed Ni–Co sample. All scale bars are 500 nm. (a) DF image collected using forescatter detectors, dominated by thickness contrast. (b) ODF image highlighting orientation variations. (c) TKD pattern quality map of the same area. (d) TKD orientation map (inverse pole figure *z*-direction colouring), with high-angle boundaries in black, low-angle boundaries in grey and coincident site lattice boundaries in colours. (e) EDS element map showing Co Kα X-ray counts. (f) EDS element map showing Ni Kα X-ray counts. (g) Mixed EDS map, showing Ni-rich regions in red and Co-rich regions in white. (h) Mixed EDS map overlain by TKD boundary map (high-angle boundaries in black, Σ3 CSL boundaries in purple, Σ11 CSL boundaries in green). Arrows correspond to boundaries highlighted in the text. (For interpretation of the references to colour in this figure legend, the reader is referred to the web version of this article.)

The EDS element maps for Co and Ni (Fig. 6e and f, respectively) appear very similar and are dominated by the thickness variations: the thicker the sample the higher the counts are for each characteristic X-ray energy. However, if we mix the element maps for both Ni and Co, with high Ni concentrations in red and high Co concentrations in white, we can see (Fig. 6g) that the Ni appears to be clearly concentrated along boundaries. This boundary Ni enrichment has been confirmed by subsequent TEM EDS line profiles. However, not all boundaries appear to be enriched in Ni. An overlay of the chemical variations onto a boundary map is shown in Fig. 6g, in which it is clear that some high-angle boundaries are enriched in Ni (long black arrows), but many of the CSL boundaries (black filled triangles) do not correspond with Ni enrichment. In addition, other high-angle boundaries (white filled triangles) also do not correspond to Ni enrichment. The relationship between crystallographic boundaries and chemical enrichment is best studied in the thinner (upper) part of this area: in the thicker regions the chemical variations are less distinct.

4. Discussion

The results presented in the previous section provide a compelling argument for the effectiveness of the SEM-TKD technique for characterizing a range of challenging, deformed samples. As stated earlier, the aim of this paper is to provide case studies illustrating the suitability of TKD for routine characterization of samples that would be impossible using conventional EBSD in SEM. In this section we will consider the key aspects of the technique, namely imaging, resolution (spatial and angular), integration with EDS, potential difficulties and a look at applications in the field of materials science.

4.1. Imaging

Convincing examples of the use of forescatter detectors for imaging electron transparent samples are provided here. It is clear that these detectors are extremely useful and versatile when setting up for subsequent TKD analyses. The DF images provide a clear indication of thickness variations in the sample, as well as good density contrast (although this is not applicable to the samples studied in this contribution), and can be used to identify suitably thin areas of the sample that would be ideal for high resolution TKD analyses. Mixing positive and inverted signals from the individual FSD diodes results in very clear ODF images that give a broad overview of the grain structure of the sample. The signal in this mode is relatively weak, as it only shows variations between the two diodes that are due to channelling or diffraction effects. In addition, the whole thickness of the sample contributes to the signal, and so for regions that have grain sizes smaller than the thickness, two or more grain orientations will contribute to the signal and the image quality will not be as good. For this reason it is hard to pick out the individual grains in the nanocrystalline matrix in the Cu sample (Fig. 2b), but extremely narrow twin domains in the coarser grains can be clearly picked out. These ODF images are hardest to interpret in heavily deformed samples in which the individual grains contain significant orientation spread. An example of this is in the Ni–Co sample (Fig. 6b). Despite some of the grains being relatively large (e.g. 250 nm wide and over 1 μm long), the ODF image does not show the grains clearly, as each grain has significant internal contrast changes due to the orientation variations. In coarser grained and less heavily deformed samples the ODF images clearly show dislocation structures and we have used this imaging technique with success on a wide range of TEM samples. In general, the DF and ODF images from the FSD system are extremely useful and are an invaluable tool to accompany the TKD measurements.

A direct comparison with TEM DF imaging is quite difficult. The scattering angle is dependent on both the insertion position of the detector as well as the working distance, but in our normal operating position (specimen to detector distance ~15 mm) the angle is typically in the range 300–500 mrad. This is significantly greater than when imaging using high-angle annular dark field (HAADF) detectors with TEM, but the lower accelerating voltage used in SEM will increase the scattering from the same sample thickness. In addition, the solid angle (i.e. the collection efficiency) of the two set-ups is broadly similar.

4.2. Resolution

The biggest single advantage of SEM-TKD compared with conventional EBSD is the gain in spatial resolution. Previous studies [27,28,38,39] indicated a true spatial resolution on the scale 5–10 nm, with potentially even better effective resolution on some samples (due to the ability of the EBSD software to deconvolve overlapping TKD patterns from adjacent grains). These figures are approximately an order of magnitude better than conventional EBSD, even considering a recent focus on lower accelerating voltage EBSD studies [26]. In addition, previous studies of TKD indicate that the signal predominantly originates from the lower surface of the sample, and not from the full thickness [27,39]. The fact that we can resolve 10–30 nm diameter grains in an 80 nm thick Cu sample (see Fig. 2c and d) is evidence for this reduced pattern origin volume. It is likely that the high scattering angles required to project Kikuchi bands onto the EBSD detector, coupled with the significantly increased electron path lengths through the sample for those electrons scattered in the upper half of the sample, is the dominant cause of this pattern origin. It is simple to calculate the expected through sample path lengths for electrons scattered at different distances from the lower surface of the sample, and to look at how these lengths vary for different positions on the phosphor screen. For the sample–detector geometry used in this study the electrons originating 40 nm from the lower surface of the sample will have a path length of 45 nm to reach the

lowermost part of the phosphor screen, and a path length of over 120 nm to reach the upper part of the phosphor screen. For electrons scattered 80 nm from the lower sample surface these values increase to 90 nm and over 250 nm, respectively. Clearly, the increase in through sample path length greatly reduces the chance of the scattered (and diffracted) electrons escaping the sample without further elastic or inelastic scattering events, and so are unlikely to contribute significantly to the resulting TKD pattern.

A result of this geometric analysis is that the diffracted signal that reaches the upper part of the phosphor screen is likely to originate much closer to the lower surface of the sample and will therefore be dominated by a signal from a smaller interaction volume. This would suggest that improved spatial resolution may be achievable by retracting the EBSD detector and maximizing the scattering angle required for projection of the TKD pattern. However, this conclusion has yet to be tested properly, and would likely result in significantly slower analyses with a subsequent increase in drift and contamination, as well as broadening of the Kikuchi bands and a reduction in the diffraction pattern solid angle, all of which would reduce indexing success.

An additional benefit of the high spatial resolution of the TKD technique is the ability to collect good diffraction patterns from samples with high dislocation densities. The spread of orientations across a small volume can prevent successful analyses using conventional EBSD, so reducing the pattern source volume is highly beneficial. Both the Ti and the Ni–Co samples shown here could not be analysed successfully using EBSD, yet were relatively easily measured using TKD. The lower limit for dislocation densities in this Ti sample, as indicated by the WBV magnitudes in Fig. 5c, is in the range of 10^{14}–10^{15} m^{-2}, even in the middle of grains and subgrains. Studies of other deformed samples using this technique have typically only shown these sort of magnitudes associated with dislocation arrays (i.e. low-angle boundaries) [37].

The angular resolution of the TKD technique is essentially similar to that of conventional EBSD (i.e. in the order of 0.5° or better on individual measurements). However, the unusual projection geometry of the TKD patterns results in relatively wide Kikuchi bands in the lower part of the pattern and this, in conjunction with the pronounced excess and deficient Kikuchi lines, can cause poor band detection using the standard Hough transform. The result is that the angular resolution in many of these datasets is approximately 1° for each measurement, although improvements to the band detection or the activation of advanced pattern fitting algorithms can reduce this to the range typical for conventional EBSD.

4.3. Integration with EDS

The ability to be able to measure the chemistry of a sample simultaneously with crystallographic characterization has been a major reason for the growth of the EBSD technique in recent years. The fact that we can also achieve this simultaneously with TKD analyses is similarly beneficial. In addition, the thin samples and the high accelerating voltages result in significantly improved spatial resolution compared with EDS bulk measurements. The results from the Ni–Co sample indicate a spatial resolution in the order of 50 nm or better, certainly good enough to resolve element enrichment along grain boundaries. However, there exist significant challenges. Firstly, EDS systems attached to scanning electron microscopes are generally configured for bulk sample quantification, using variations of the ZAF matrix corrections [40]. For accurate quantitative measurements on TEM foils such systems need to be able to switch to TEM correction techniques such as the Cliff–Lorimer ratio technique [41]. For a number of commercial systems this would involve the purchase of additional options, making it a less attractive option. Secondly, the sample holder used to mount the TEM foils can be a source of significant background fluorescence. The purpose built TKD holder shown in Fig. 1 is tapered in order to minimize the background X-rays but, even so, there remains a considerable background Al X-ray signal originating from the holder itself. Thirdly, the X-ray count rate during TKD analyses can be relatively low, occasionally resulting in fewer than 20 X-rays per measured point. This number can be increased by slowing down the analysis or by increasing the beam current (for example by using a larger aperture in the electron column), however, both approaches can lead to increased contamination, drift or sample damage. A better solution is to use a large area EDS detector. The results shown in this paper utilize a 20 mm^2 detector typically giving >50 X-rays per point, but detectors as large as 150 mm^2 are commercially available and would provide significantly better X-ray data with no penalty on speed or TKD data quality.

Despite these technical issues, the results of integrated TKD and EDS analysis of the Ni–Co sample shown in Fig. 6 illustrate the potential of this technique for correlating element segregation with crystallographic boundary properties with high spatial resolution. It is clear that a number of high-angle boundaries are significantly enriched in Ni and that special boundaries (such as CSL boundaries) generally have no noticeable segregation. However, there are a number of high-angle boundaries that either do not show significant element segregation or the Ni concentration appears to be laterally displaced from the position of the boundary in the TKD orientation map. The former case may well indicate differing boundary origins and will need more detailed examination in a future publication. The latter case is likely to be caused by differences in the boundary plane orientation; the TKD data predominantly originates from the lower surface of the sample, whereas the X-ray data comes from the whole thickness. This means that boundaries oriented at a shallow angle to the sample surface will have the boundary location in the orientation map displaced from the dominant chemical signature associated with any element segregation.

4.4. Technical challenges

TKD analyses of highly deformed or nanocrystalline materials are not as straightforward as conventional EBSD analyses of coarser grained or less deformed samples. The stability of the system is very important, and this includes the stability of the electron beam as well as the mechanical and thermal stability of the sample itself. For high-magnification analyses with step sizes of 5 nm or less (such as in Figs. 2 and 3) it was generally necessary to allow the system to stabilize for a period of 2 h or more. This reduced noticeable mechanical drift of the stage and improved vacuum levels in the specimen chamber, thereby reducing contamination of the sample during subsequent analyses. The best results were achieved when the sample had been in the scanning electron microscope overnight, with the electron beam scanning a thicker part of the TEM foil. Despite this, occasional fluctuations in the temperature of the laboratory or, more noticeably, the water cooling system for the scanning electron microscope caused noticeable instabilities in the electron beam. These were of the order of a few tens of nanometres every 5–10 min: large enough to be seen in TKD orientation maps, but not noticeable during conventional EBSD work. Although data has been collected with step sizes of 2 nm or less [28], the most successful larger analyses have been completed with step sizes of 4 nm or larger: the respective drop in electron current density reduces the sample damage and contamination, and the increased speed of scanning minimizes the effect of any drift.

Sample preparation was also a significant challenge. The relatively low acceleration voltage used for TKD work (compared with standard TEM analyses) necessitates thin samples (i.e. under 150 nm thickness). Although indexable TKD patterns can be acquired from regions thicker than 1 μm, the increased lateral scattering of the electron beam dramatically reduces the effective spatial resolution of the technique. In addition, the X-ray counts during simultaneous EDS mapping are directly related to the sample thickness, as visible in Fig. 6. The best results are achieved on samples that have a large thin area with minimal variations in the thickness: for some samples suitable preparation has only been achievable using a focused ion beam scanning electron microscope.

4.5. Applications

TKD orientation mapping is quickly becoming an indispensible tool for the characterization of highly deformed UFG and nanocrystalline materials. The accessibility of the technique to any laboratory with a FEG scanning electron microscope equipped with an EBSD system is likely to result in it becoming more common than comparable advanced automated TEM diffraction techniques. Naturally the main applications will be where the spatial resolution of conventional EBSD is insufficient to resolve the microstructure, such as in UFG and nanocrystalline materials and in highly deformed materials, as demonstrated in this paper. The ability to collect simultaneous chemical information with sub-100 nm resolution makes TKD with EDS a unique combination for correlating orientation and misorientation data with chemical segregation. It cannot compete with high-resolution TEM or atom probe tomography (APT) for resolution, but has the advantage of both statistics and automation, and is an ideal technique for identifying relationships between chemistry and crystallography.

Further developments are likely to include routine analyses of tips for APT. The greatest challenge is to minimize carbon contamination during the scanning of tips, as this decreases the likelihood of a successful APT analysis, although early results in this correlative field are encouraging. The technique may also be used for rapid overall mapping of the distribution and orientations of phases within thin specimens prior to detailed TEM studies that utilize diffraction, high-resolution imaging or sophisticated microanalytical work. There is also likely to be significant use of TKD to measure lattice strains and dislocation densities using high resolution pattern correlation techniques [42]. The smaller pattern source volume allows the collection of very sharp high-quality Kikuchi patterns that can be used for pattern correlation in samples that are highly deformed or strained, something that was challenging or impossible with conventional EBSD. The additional space in a scanning electron microscope chamber also makes it relatively simple to design and carry out in situ deformation (and heating) experiments in conjunction with TKD, although contamination or sample damage caused by repeated scanning may be an issue that is difficult to resolve.

5. Conclusions

This study shows how the new technique of SEM-TKD can be used to characterize UFG or nanocrystalline materials that have undergone deformation. The salient issues can be summarized as follows.

1. TKD is a rapidly developing technique that utilizes conventional EBSD hardware and software in a scanning electron microscope to characterize the microstructures of electron transparent samples.
2. Forescatter detectors, mounted below the EBSD detector phosphor screen, can be used to generate high-quality DF and ODF images of TEM samples.
3. The high spatial resolution of the TKD technique (<10 nm) enables effective orientation mapping of nanocrystalline samples, with mean grain sizes significantly below 50 nm.
4. The high spatial resolution also allows routine characterization of highly deformed materials, including those that have undergone room temperature severe plastic deformation and have extremely high dislocation densities.

5. Combining TKD with simultaneous EDS measurements allows the correlation of elemental segregation with grain boundary properties on the scale 10–50 nm.

Acknowledgements

The authors are grateful for the assistance of technical staff at the Australian Centre for Microscopy and Microanalysis at the University of Sydney, a node of the Australian Microscopy and Microanalysis Research Facility, and in particular Adam Sikorski for his help with sample preparation. Andrew McVicar and Gemma Thompson at the School of Chemistry, the University of Sydney, are thanked for facilitating, designing and constructing the TKD sample holder used for this research. Scott Sitzman (Oxford Instruments Nanoanalysis) is thanked for discussions relating to TKD and the use of forescatter detectors, including the suggestion to invert one of the diode signals. K.J.H. would like to acknowledge the support of The US Department of Energy, Office of Basic Energy Sciences (DE-FG02-07ER46437) and National Science Foundation (DMR-1008156). J.M.C. and X.L. acknowledge support from the Australian Research Council.

References

[1] Huang Y, Langdon T. Mater Today 2013;16:85–93.
[2] Artz E. Acta Mater 1998;46:5611–26.
[3] Meyers MA, Mishra A, Benson DJ. Prog Mater Sci 2006;51:427–556.
[4] Liddicoat PV, Liao XZ, Zhu YT, Zhao YH, Lavernia EJ, Murashkin MY, et al. Nat Commun 2010;1:1–7.
[5] Schiøtz J, Jacobsen KW. Science 2003;301:1357–9.
[6] Kumar KS, Swygenhoven H, Suresh S. Acta Mater 2003;51:5743–74.
[7] Boyce BL, Padilla II HA. <http://link.springer.com/article/10.1007/s11661-011-0708-x/fulltext.html>.
[8] Suryanarayana C, Koch CC. Hyperfine Interact 2000;130:5–44.
[9] Hernando A. J Phys Condens Matter 1999;11:9455–82.
[10] Bai XM, Voter AF, Hoagland RG, Nastasi M, Uberuaga BP. Science 2010;327:1631–4.
[11] Valiev RZ, Islamgaliev RK, Alexandrov IV. Prog Mater Sci 2000;45:103–89.
[12] Zehetbauer M, Grossinger R, Krenn H, Krystian M, Pippan R, Rogl P, et al. Adv Eng Mater 2010;12:692–700.
[13] Iwahashi Y, Wang JT, Horita Z. Scripta Mater 1996;35:143–6.
[14] Zhilyaev AP, Langdon TG. Prog Mater Sci 2008;53:893–979.
[15] Markushev MV, Bampton CC, Murashkin MY, Hardwick DA. Mater Sci Eng A 1997;234:927–31.
[16] Valiev RZ, Alexandrov IV, Zhu YT, Lowe TC. J Mater Res 2002;17:5–8.
[17] Rauch EF, Portillo J, Nicolopoulos S, Bultreys D, Rouvimov S, Moeck P. Z Kristallogr 2010;225:103–9.
[18] Kobler A, Kashiwar A, Hahn H, Kubel C. Ultramicroscopy 2013;128:68–81.
[19] Zhao YH, Liao XZ, Cheng S, Ma E, Zhu YT. Adv Mater 2006;18:2280–3.
[20] Wu X, Xu W, Xia K. Mater Sci Eng A 2008;493:241–5.
[21] Humphreys FJ, Brough I. J Microsc 1999;195:6–9.
[22] Dingley D. J Microsc 2004;213:214–24.
[23] Humphreys FJ. Scripta Mater 2004;51:771–6.
[24] Prior DJ, Trimby PW, Weber UD, Dingley DJ. Mineral Mag 1996;60:859–69.
[25] Chen D, Kuo J-C, Wu W-T. Ultramicroscopy 2011;111:1488–94.
[26] Steinmetz DR, Zaefferer S. Mater Sci Technol 2010;26:640–5.
[27] Keller RR, Geiss RH. J Microsc 2012;245:245–51.
[28] Trimby PW. Ultramicroscopy 2012;120:16–24.
[29] Tugcu K, Sha G, Liao XZ, Trimby PW, Xia JH, Murashkin MY, et al. Mater Sci Eng A 2012;552:415–8.
[30] Kacher J, Elizaga P, House SD, Hattar K, Nowell M, Robertson IM. Mater Sci Eng A 2013;568:49–60.
[31] Sun JL, Trimby PW, Si X, Liao XZ, Tao NR, Wang JT. Scripta Mater 2013;68:475–8.
[32] Sun JL, Trimby PW, Yan FK, Liao XZ, Taod NR, Wang JT. Scripta Mater 2013;69:428–31.
[33] Cao Y, Wang YB, Figueiredo RB, Chang L, Liao XZ, Kawasaki M, et al. Acta Mater 2011;59:3903–14.
[34] Zhao WS, Tao NR, Guo JY, Lu QH, Lu K. Scripta Mater 2005;53:745–9.
[35] Zhang Y, Tao NR, Lu K. Acta Mater 2008;56:2429–40.
[36] Qin L, Lian J, Jiang Z, Wang G, Jiang Q. J Mater Res 2010;25:401–5.
[37] Wheeler J, Mariani E, Piazolo S, Prior DJ, Trimby P, Drury MR. J Microsc 2009;233:482–94.
[38] Brodusch N, Demers H, Gauvin R. J Microsc 2013;250:1–14.
[39] Geiss RH, Rice KP, Keller RR. Micros Today 2013;21:16–20.
[40] Heinrich KFJ, Newbury DE, editors. Electron probe quantitation. New York: Plenum Press; 1991.
[41] Cliff G, Lorimer GW. J Microsc 1975;103:203–7.
[42] Wilkinson AJ, Dingley DJ, Meaden GM. Microsc Microanal 2005;11:520–1.